frontiers | Frontiers in Energy Research

TYPE Original Research
PUBLISHED 30 May 2024
DOI 10.3389/fenrg.2024.1376714

OPEN ACCESS

EDITED BY
Xiongbo Duan,
Central South University, China

REVIEWED BY
Nihat Ozturk,
Gazi University, Türkiye
Tao Qin,
Hunan University, China

*CORRESPONDENCE
Weiqiang Liao,
wq_liao@jmu.edu.cn

RECEIVED 26 January 2024
ACCEPTED 22 April 2024
PUBLISHED 30 May 2024

CITATION
Dong X, Wang H, Zhang C, Yu W, Yang R, Xiao L, Liao W and Luo C (2024), The power flow algorithm for AC/DC microgrids based on improved unified iteration method.
Front. Energy Res. 12:1376714.
doi: 10.3389/fenrg.2024.1376714

The power flow algorithm for AC/DC microgrids based on improved unified iteration method

Xin Dong[1], Haibin Wang[2], Changkun Zhang[1], Wanneng Yu[1,3], Rongfeng Yang[1,3], Longhai Xiao[1,3], Weiqiang Liao[1,3,4]* and Chenghan Luo[1]

[1]School of Marine Engineering, Jimei University, Xiamen, China, [2]Department of Naval Architecture, Ocean and Marine Engineering, University of Strathclyde, Glasgow, United Kingdom, [3]Marine Engineering College and Key Laboratory of Fujian Province Marine and Ocean Engineering, Jimei University, Xiamen, China, [4]Innovation Laboratory for Sciences and Technologies of Energy Materials of Fujian Province, Xiamen, China

In response to the complexity of the Jacobian matrix inversion process in the power flow algorithm for AC/DC microgrids, leading to large memory requirements and susceptibility to convergence issues, a novel power flow algorithm based on an improved unified iteration method for AC/DC microgrids is proposed. Firstly, the fundamental equations of the unified iteration method and the characteristics of DC systems are analyzed. The reactive power correction terms and voltage phase correction differences are removed from the modified equations of the unified iteration method, and result in a reduction in the order of the Jacobian matrix in the power flow algorithm. Subsequently, the improved IEEE 11-node system is subjected to simulation verification to attain precise power flow solutions for hybrid AC/DC microgrids. The theoretical analysis identifies the main influencing parameters of active and reactive power errors and assesses their impact factors. Finally, experimental validation of the improved power flow algorithm is carried out on a physical platform, clarifying the applicability range of the proposed method. The research results indicate that within allowable error margins, the proposed approach reduces the difficulty of Jacobian matrix inversion, resulting in an 80% increase in computational speed compared to the unified iteration method. It is suitable for microgrid systems with short electrical distances and small magnitudes of node voltage amplitudes and phase differences.

KEYWORDS

hybrid ac/dc microgrid, power flow algorithm, system characteristics, unified iteration method, matrix reduction

1 Introduction

In the context of "carbon peak" and "carbon neutrality," the penetration of distributed generation technology in the power grid is gradually increasing, and microgrids have become an effective form of utilizing distributed generation technology (Song et al., 2021; Zou et al., 2022). Hybrid AC/DC microgrids, combining the advantages of both AC and DC microgrids, have become an important direction in the development of microgrid technology. However, there exist complex coupling relationships between AC and DC within the system. Therefore, how to systematically analyze AC/DC microgrids and ensure their safe and stable operation has become a focal research area for scholars worldwide (Liu K. et al., 2019; Hameed et al., 2019; Yang et al., 2019).

Power flow analysis, as one of the fundamental tools for microgrid analysis, its mathematical essence involves solving a set of multivariate nonlinear equations through iterative computations to determine parameters such as voltage, phase angle, and power at various nodes (or buses) within the grid. Power flow analysis is employed to ascertain load distribution, voltage stability, line power losses, and flow distribution of components such as generators, transformers, and transmission lines within the power system (Guoqing et al., 2017; Pengfei, 2022), plays a crucial role in microgrid planning, stability calculations, and fault analysis (Bajpai, 2023; Heidary et al., 2023; Huang et al., 2023; Li et al., 2023). Currently, commonly used power flow calculation methods for AC/DC microgrids include the unified iteration method (UIM) and the alternate iteration method (Nejabatkhah et al., 2019; Song et al., 2023). The alternate iteration method separately solves power flow for AC and DC subsystems, providing fast calculation speeds but relatively lower convergence accuracy. On the other hand, the unified iteration method extends the dimension of the Jacobian matrix by introducing DC variables, allowing for the joint solution of variables in AC and DC systems. However, this increases the order of the Jacobian matrix, requiring matrix decomposition in each iteration, thereby adding to the overall computation time (Wang et al., 2018). Therefore, reducing computational complexity and time in the power flow calculation process while ensuring accuracy has become an important aspect of research on power flow calculation in hybrid AC/DC microgrids.

To enhance the efficiency of AC/DC microgrid power flow calculations, related research has primarily focused on improving existing methods. Reference (Liu et al., 2021) proposed a control mode for distributed grids participating in voltage and frequency regulation based on the Newton-Raphson method. On this basis, it introduced a sequential algorithm framework for handling coupling relationships between AC and DC microgrids. Using an improved Newton-Raphson sub-algorithm, it iteratively solved power flow for hybrid AC/DC microgrids. Reference (Ju et al., 2022) presented a fully Distributed Power Flow (DPF) method, transforming nonsmooth constraints into smooth functions. It employed a two-level Augmented Lagrangian Alternating Direction Inexact Newton (ALADIN) method with second-order convergence speed to convert the DPF problem into a distributed step-size optimization problem. By exchanging microgrid boundary information, it achieved accurate power flow results and improved convergence speed and accuracy through the second-level step-size optimization. Reference (Chen et al., 2017) established a steady-state power flow model for a Droop-type distributed power source and AC/DC inverter. It applied a sequence component conversion based on voltage symmetry at the grid connection point and used a sequence current compensation method to decouple the AC subgrid into three-sequence networks, solving them in parallel and further reducing the solution capacity.

While the above literature has improved computational accuracy and speed through enhancements to existing methods, it does not address the impact of DC system characteristics on power flow calculation equations. To address this gap, this paper first comprehensively considers DC system characteristics and proposes an AC/DC microgrid power flow algorithm based on the unified iteration method. This resolves the issues of long computation times and high computational capacity associated with the unified iteration power flow calculation method. Subsequently, through simulation experiments on the IEEE 11-node system, the effectiveness and high computational efficiency of the proposed algorithm are validated. The study identifies the factors and extent of error generation under different conditions. Finally, experimental verification on a 30 kW load and 70 kW load is conducted on the experimental platform, confirming the feasibility of the improved algorithm.

2 The power flow algorithm for AC/DC systems and its improvement

In an AC/DC microgrid, which includes both AC and DC lines, the selection of DC lines leads to variations in system structure and operational modes. Consequently, there are differences in the equivalent models and DC equations.

Taking a two-terminal bipolar DC transmission system as an example, the selected DC line model is systematically modeled (Yang et al., 2021; Zhu et al., 2022), resulting in the equivalent circuit of the DC system as illustrated in Figure 1:

From the equivalent circuit shown in Figure 1, the expressions for the main parameters of the DC line can be obtained as follows:

$$I_d = \frac{3\sqrt{2}E_r \cos\alpha/\pi - 3\sqrt{2}E_i \cos\beta/\pi}{d_{xr} + R_1 + d_{xi}} \tag{1}$$

$$\begin{cases} P_{dr} = U_{dr} I_d \\ P_{di} = U_{di} I_d = P_{dr} - I_d^2 R_1 \end{cases} \tag{2}$$

$$\begin{cases} U_{dr} = 3\sqrt{2}\, E_r \cos\alpha/\pi - I_d d_{xr} \\ U_{di} = 3\sqrt{2}\, E_i \cos\beta/\pi + I_d d_{xi} \\ U_{dr} = U_{di} + I_d R_i \end{cases} \tag{3}$$

Eqs 1–3 form the main parameter equations for the two-terminal bipolar DC transmission system.

For a hybrid AC/DC system model with a total of n nodes, let the number of DC nodes be n_d, and the number of AC nodes be $n_a = n - n_d$, To facilitate the construction of correction equations, the nodes of the system are numbered as follows: the first n_a nodes are labeled as AC nodes, and the remaining n_d nodes are labeled as DC nodes.

For a pure AC system with n_a nodes, the power equations and correction equations in the polar coordinate form of the Newton-Raphson method are expressed as Eqs 4, 5, respectively.

$$\begin{cases} \Delta P_i = P_i - U_i \sum_{j=1}^{n} U_j \left(G_{ij} \cos\delta_{ij} + B_{ij} \sin\delta_{ij} \right) \quad i = 1, 2, ..., n_a \\ \Delta Q_i = Q_i - U_i \sum_{j=1}^{n} U_j \left(G_{ij} \sin\delta_{ij} - B_{ij} \cos\delta_{ij} \right) \quad i = 1, 2, ..., n_a \end{cases} \tag{4}$$

$$\begin{pmatrix} \Delta P_a \\ \Delta Q_a \end{pmatrix} = -\begin{pmatrix} H_{aa} & N_{aa} \\ M_{aa} & L_{aa} \end{pmatrix} \begin{pmatrix} \Delta\delta_a \\ \Delta U_a / U_a \end{pmatrix} = -[J] \begin{pmatrix} \Delta\delta_a \\ \Delta U_a / U_a \end{pmatrix} \tag{5}$$

Where the subscript 'a' represents AC variables; $\Delta P_a = [\Delta P_1\, \Delta P_2 \cdots \Delta P_{n_a}]^T$, $\Delta Q_a = [\Delta Q_1\, \Delta Q_2 \cdots \Delta Q_{n_a}]^T$, H_{aa}, N_{aa}, M_{aa}, L_{aa} are the sub-matrix of partial derivatives of the quantity to be corrected with respect to the correction variables, such as $H_{aa} = \partial\Delta P_a / \partial\delta_a$, $N_{aa} = (\partial\Delta P_a / \partial U_a) \times U_a$。

The power equations of the UIM are established based on the power equations of the AC system, with the inclusion of DC variables (Peng et al., 2017; Liu K et al., 2019; Lin et al., 2020; Wang et al., 2023). Combining the proposed DC model, the power

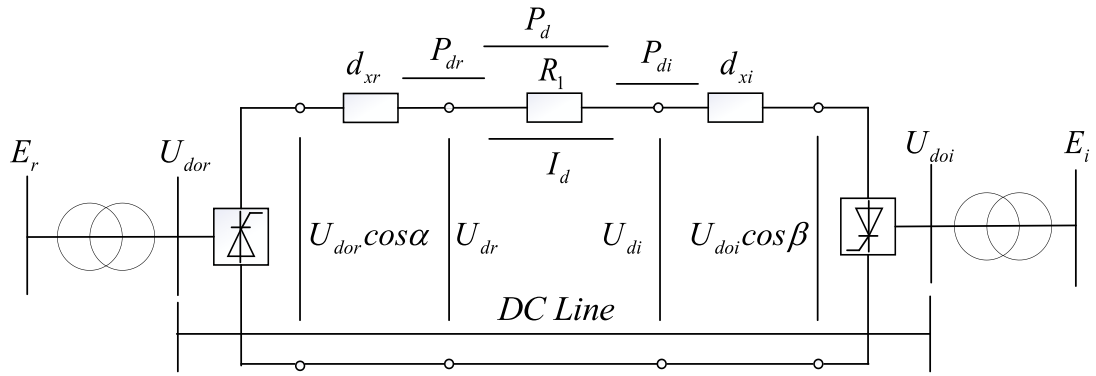

FIGURE 1
Steady-state model of two-terminal bipolar DC transmission system.

equation for the hybrid AC/DC system is obtained by introducing DC variables into Eq. 4, as shown in Eq. 6:

$$\begin{cases} \Delta P_i = P_i - U_i\sum_{j=1}^{n}U_j\left(G_{ij}\cos\delta_{ij} + B_{ij}\sin\delta_{ij}\right) \\ \pm U_{dk}I_{dk}, i = n_d + k, k = 1, 2, \cdots n_d \\ \Delta Q_i = Q_i - U_i\sum_{j=1}^{n}U_j\left(G_{ij}\sin\delta_{ij} - B_{ij}\cos\delta_{ij}\right) \\ \pm U_{dk}I_{dk}\tan\varphi_k, i = n_d + k, k = 1, 2, \cdots n_d \end{cases} \tag{6}$$

Where the positive and negative signs represent the inverter and rectifier, respectively.

Considering the presence of DC variables in the mixed AC/DC system, in Eq. 5, active power and reactive power imbalance terms for the DC nodes, as well as phase difference and voltage difference, are introduced. From Eq. 6, it can be observed that the correction equations introduce new variables U_{dk}, I_{dk}, φ_k . At this point, the number of variables exceeds the number of equations. According to the theory of the boundedness of solutions in a linear space, it is necessary to supplement the correction equations with new equations to ensure that the number of equations is greater than or equal to the number of variables.

Combining Eqs 1–3, supplement the parameter equation ΔZ_p and control equation ΔZ_p for the DC system in the quantity to be corrected, and express them uniformly as ΔZ.

Rearranging Eq. 3 and forming the parameter equation ΔZ_p for the DC system is shown in Eq. 7 (Chen et al., 2019; Lee et al., 2020):

$$\Delta Z_p = \begin{cases} U_{dr} - 3\sqrt{2}E_r\cos\alpha/\pi + I_d d_{xr} = 0 \\ U_{di} - 3\sqrt{2}E_i\cos\beta/\pi - I_d d_{xi} = 0 \\ U_{dr} - R_i I_d - U_{di} = 0 \end{cases} \tag{7}$$

The main control equation for the DC system is expressed as Eq. 8:

$$\Delta Z_c = \begin{cases} P - P_s = 0 \\ \beta - \beta_s = 0 \\ \alpha - \alpha_s = 0 \\ I_d - I_s = 0 \\ U_d - U_s = 0 \\ K_r - K_s = 0 \\ K_i - K_s = 0 \end{cases} \tag{8}$$

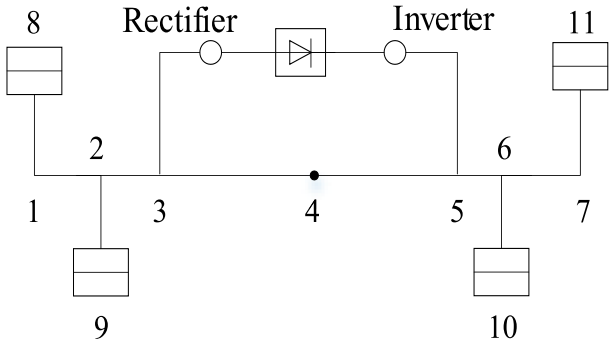

FIGURE 2
Improved structure diagram of IEEE 11 system.

Where the variables with subscript's' represent the system rated values; ΔZ_c is determined based on the specific control method.

Due to the increase in the quantity to be corrected on the left side of the correction equation, and with only phase difference and voltage difference in the correction discrepancy, it is still not possible to solve the correction equation. Considering the inclusion of Eqs 7, 8 in the quantity to be corrected, and incorporating the characteristic parameters of the DC system, the correction discrepancy for the DC system is expanded by introducing the correction variable ΔX. The specific expression is shown in Eq. 9.

$$\Delta X = \left[\Delta U_d^T\ \Delta I_d^T\ \Delta K_d^T\ \Delta W^T\ \Delta\Phi^T\right]^T \tag{9}$$

The specific expressions for each variable in ΔX are shown in Eq. 10:

$$\begin{cases} \Delta U_d = \left[\Delta U_{d1}\ \Delta U_{d2}\ \Delta U_{d3}\cdots\Delta U_{dn_d}\right]^T \\ \Delta I_d = \left[\Delta I_{d1}\ \Delta I_{d2}\ \Delta I_{d3}\cdots\Delta I_{dn_d}\right]^T \\ \Delta K_T = \left[\Delta K_{T1}\ \Delta K_{T2}\ \Delta K_{T3}\cdots\Delta K_{Tn_d}\right]^T \\ \Delta W = \left[\Delta\cos\theta_{d1}\ \Delta\cos\theta_{d2}\cdots\Delta\cos\theta_{dn_d}\right]^T \\ \Delta\Phi = \left[\Delta\varphi_1\ \Delta\varphi_2\ \Delta\varphi_3\cdots\Delta\varphi_{n_d}\right]^T \end{cases} \tag{10}$$

Thus, the correction equation for the UIM in the mixed AC/DC system is:

TABLE 1 AC line parameters.

Branch number	Start node	End node	Resistance	Reactance	Branch type
1	1	2	0.0025	0.025	Line
2	1	8	0	0.0167	Transformer
3	2	3	0.001	0.01	Line
4	2	9	0	0.0167	Transformer
5	3	4	0.006	0.055	Line
6	4	5	0.006	0.055	Line
7	5	6	0.001	0.01	Line
8	6	7	0.0025	0.025	Line
9	6	10	0	0.0167	Transformer
10	7	11	0	0.0167	Transformer

TABLE 2 DC line parameters.

Node number	Control angle	Active power	DC current	Commutation reactance	DC resistance
3	0.324	0	2.203	0.015	0.04
5	0.383	1.809	2.203	0.015	0.04

TABLE 3 Comparison of calculation time.

Power flow calculation method	Calculate time/s	Number of iterations/times
UIM	0.02	5
IUIM	0.004	5

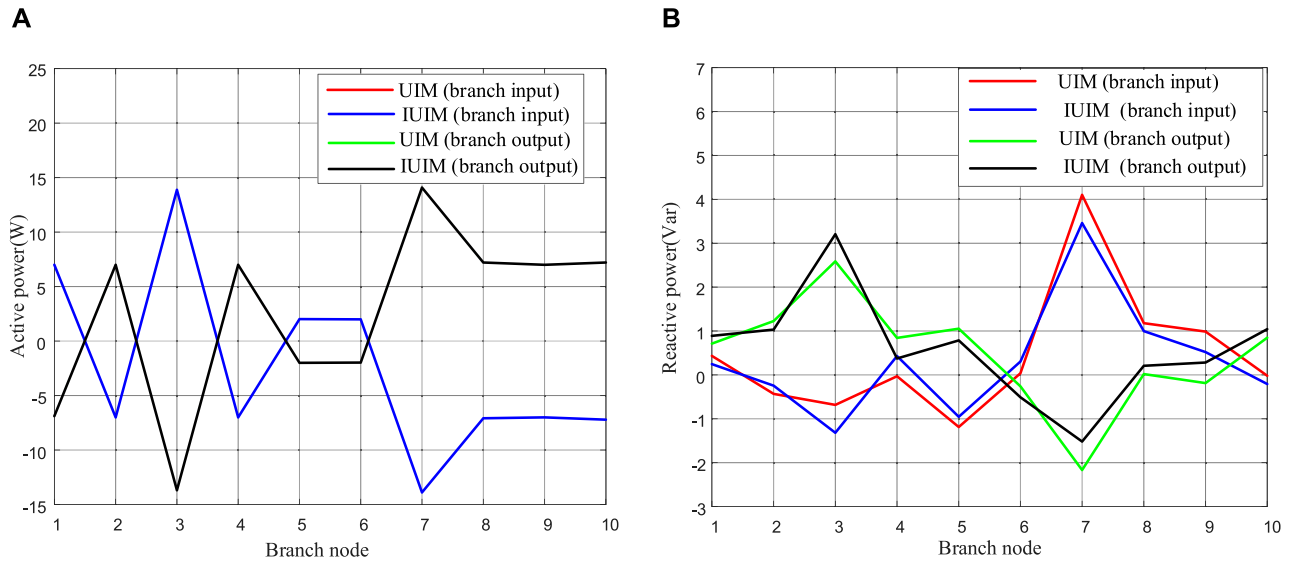

FIGURE 3
Comparison of power input and output of branch. **(A)** Active power. **(B)** Reactive power.

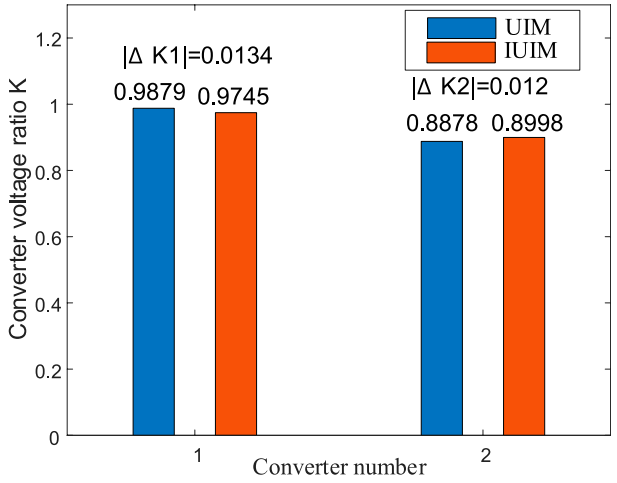

FIGURE 4
Comparison of voltage ratio of DC converter.

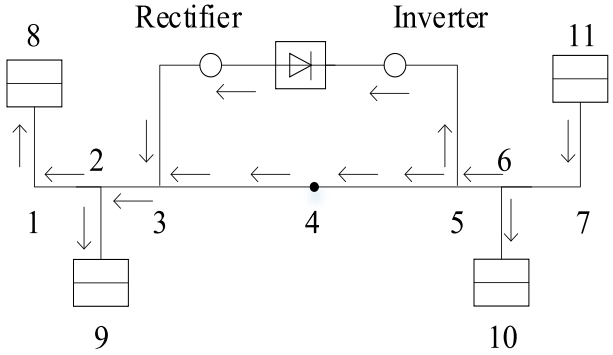

FIGURE 6
Power flow diagram of the improved IEEE11 system.

$$\begin{pmatrix} \Delta P_a \\ \Delta P_d \\ \Delta Q_a \\ \Delta Q_d \\ \Delta Z \end{pmatrix} = -\begin{pmatrix} H_{aa} & H_{ad} & N_{aa} & N_{ad} & 0 \\ H_{da} & H_{dd} & N_{da} & N_{dd} & A \\ M_{aa} & M_{ad} & L_{aa} & L_{ad} & 0 \\ M_{da} & M_{dd} & L_{da} & L_{dd} & B \\ 0 & 0 & 0 & C & D \end{pmatrix} \begin{pmatrix} \Delta\delta_a \\ \Delta\delta_d \\ \Delta U_a/U_a \\ \Delta U_d/U_d \\ \Delta X \end{pmatrix} = -[J'] \begin{pmatrix} \Delta\delta_a \\ \Delta\delta_d \\ \Delta U_a/U_a \\ \Delta U_d/U_d \\ \Delta X \end{pmatrix} \tag{11}$$

Among them, $A = \partial\Delta P_d/\partial X$; $B = \partial\Delta Q_d/\partial X$; $C = (\partial\Delta Z/\partial U_d) \times U_d$; $D = \partial\Delta Z/\partial X$; Where the elements of the sub-matrices H, N, M, and L in J' are the same as those in Eq. 5.

Compared to the Jacobian matrix J in Eq. 5, the order of the augmented Jacobian matrix J' in Eq. 11 has increased by $5\times n_d$. The increase in the order of the Jacobian matrix can complicate the process of solving the inverse matrix, potentially leading to singular values and causing non-convergence of the calculation results. Additionally, it occupies a considerable amount of computational memory and increases the power flow computation time, necessitating improvements.

In DC lines, the power factor is determined by factors $cos\,\varphi = 1$ and $Q = UIsin\varphi$. Meanwhile, only resistive loads are effective in DC circuits, and during power flow analysis, only steady-state changes need to be considered. Therefore, in DC, only active power consumption is considered, and the flow of reactive power is not taken into account. As a result, there is no need for iterative calculations for the variable ΔQ_d in the quantity to be corrected.

At the same time, when transmitting electric energy in DC form, due to the special characteristics of DC power supply, there is no induction of reactance in the line during the energy transmission process, and there is no issue of voltage phase angle. For the DC portion in the mixed AC/DC system, there is no need to consider the phase deviation $\Delta\delta_d$ in the correction discrepancy, which means

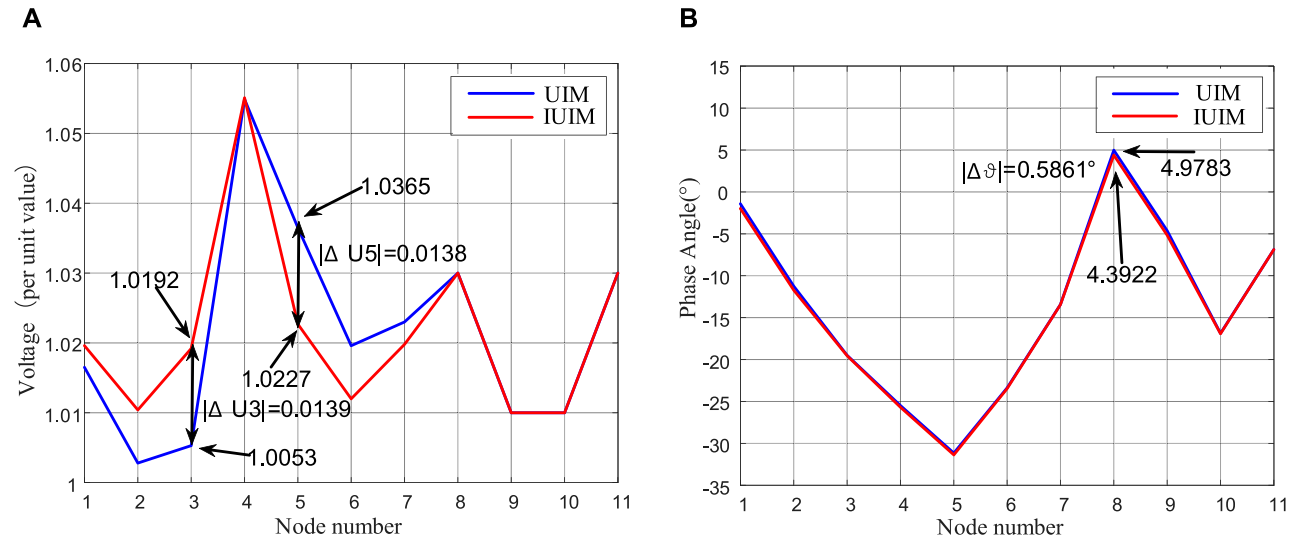

FIGURE 5
Comparison of Node Voltage Calculation Results. **(A)** Node voltage amplitude. **(B)** Node phase.

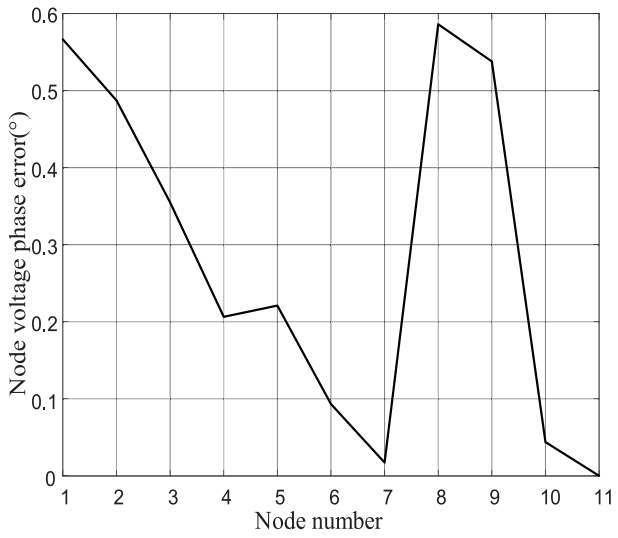

FIGURE 7
Node voltage phase error curve.

removing the variables ΔQ_d and $\Delta \delta_d$ from Eq. 11. The resulting correction equation is shown in Eq. 12:

$$\begin{pmatrix} \Delta P_a \\ \Delta P_d \\ \Delta Q_a \\ \Delta Z \end{pmatrix} = -\begin{pmatrix} H_{aa} & N_{aa} & N_{ad} & 0 \\ H_{da} & N_{da} & N_{dd} & A \\ M_{aa} & L_{aa} & L_{ad} & 0 \\ 0 & 0 & C & D \end{pmatrix} \begin{pmatrix} \Delta \delta_a \\ \Delta U_a / U_a \\ \Delta U_d / U_d \\ \Delta X \end{pmatrix} \tag{12}$$

Eq. 12 represents the expression of the corrected equation after improvement, which is the correction equation of the improved unified iteration method (IUIM).

3 Example verification

3.1 Parameter settings

The standard IEEE 11-node system is modified in this paper to form a hybrid AC/DC microgrid system, and the feasibility and computational accuracy of the proposed method are tested. The system structure is shown in Figure 2. The total number of nodes is $n = 11$, with $n_a = 9$ AC nodes and $n_d = 2$ DC nodes. Generators at nodes 8, 9, and 10 are replaced with photovoltaic sources, wind turbines, and fuel cells, treated as PV, PQ, and PV nodes, respectively. The active power output at node nine is set to $P = 7$ (per unit value), and the voltages at nodes 8 and 10 are $V_8 = 1.03$ and $V_{10} = 1.01$, respectively. Node 11 is designated as the Slack node with a voltage of $V_{11} = 1.03\angle - 0.18^\circ$. DC lines are added directly between nodes 3 and 5, with node 3 as the rectifier side and node 5 as the inverter side, while other lines are AC lines. The convergence accuracy is set to 1×10^{-4} for all calculations.

The parameters of the AC lines in the system are shown in Table 1, and the parameters of the DC lines are shown in Table 2, all represented in per unit values.

3.2 Results of the example

Comparing the computational results between the UIM and the proposed approach, the computation times are presented in Table 3. With the same convergence achieved in 5 iterations, the UIM has a computation time of 0.02 s, while the IUIM has a computation time of 0.004 s. With the same convergence accuracy, the computational speed has been improved, showing an 80% increase in speed.

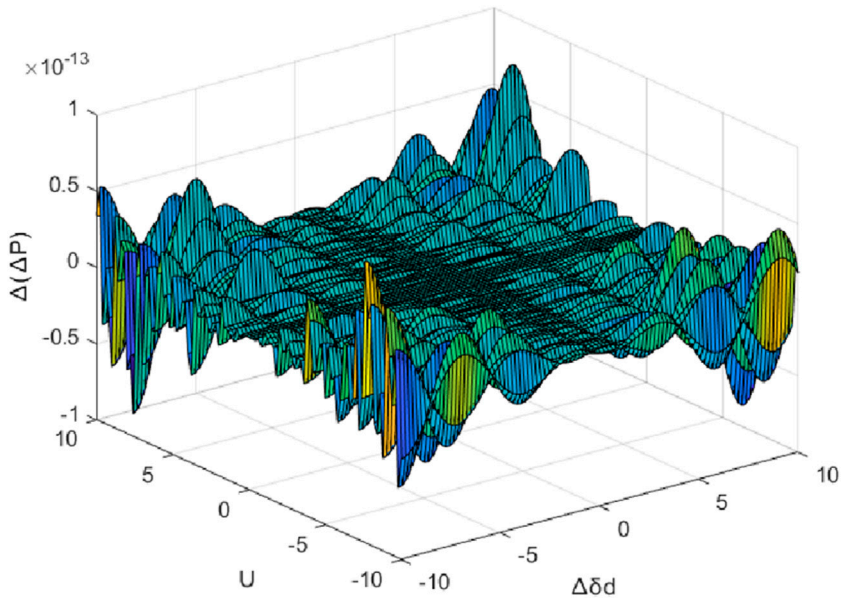

FIGURE 8
Active power error influence trend.

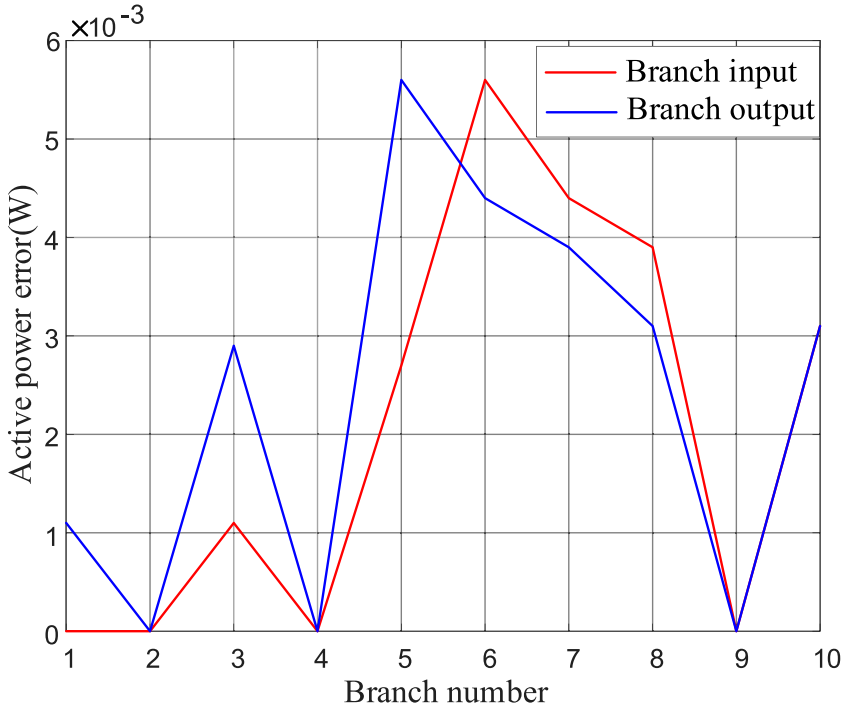

FIGURE 9
Active power error curve.

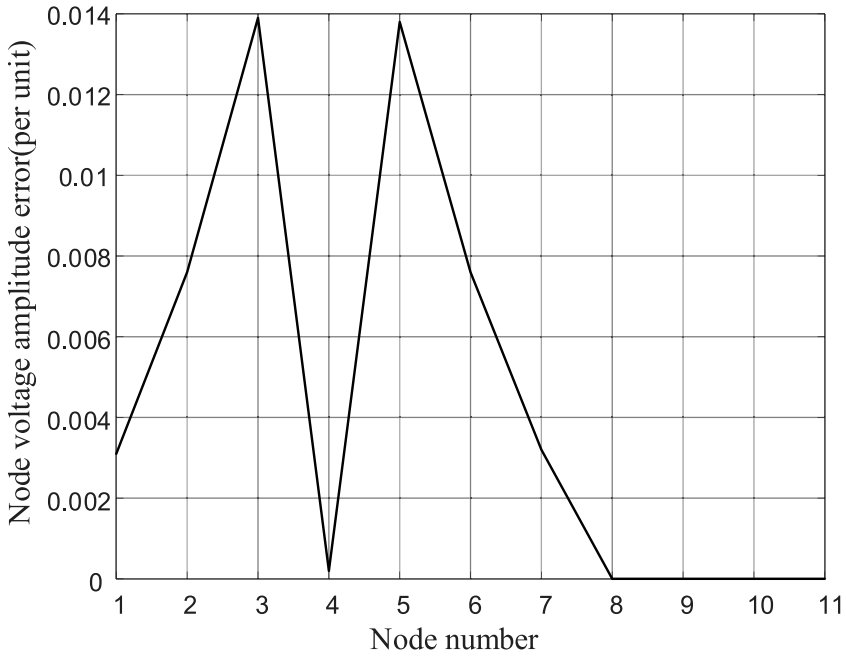

FIGURE 10
Node voltage error curve.

Comparing the injected active and reactive power of branches as shown in Figures 3A, B, the active power exhibits virtually no error. The maximum deviation for active power input (output) of branches is $|\Delta P_{\max}| = 0.0056$, with an average relative error of $\overline{|\Delta P|} = 0.00239$. For reactive power, the maximum deviation in input is $|\Delta Q_{in\max}| = 0.6419$, and in

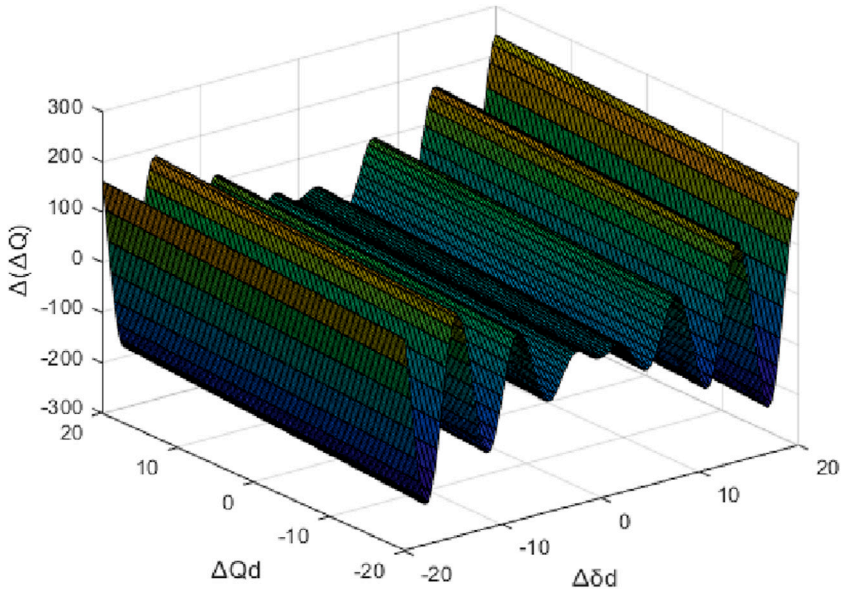

FIGURE 11
Reactive power error influence trend.

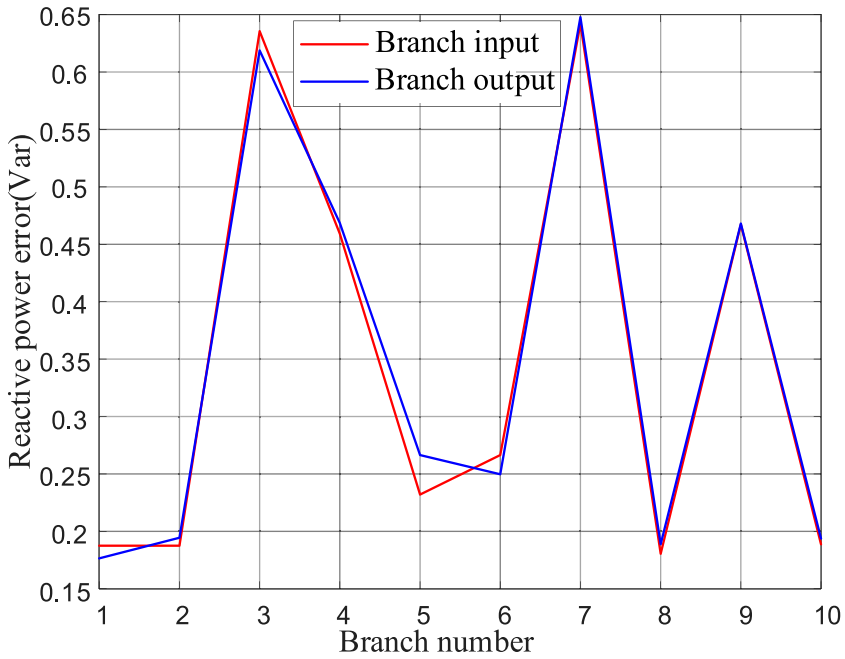

FIGURE 12
Reactive power error curve.

output is $|\Delta Q_{out\,\max}| = 0.6478$, with an average relative error of $\overline{|\Delta Q|} = 0.11564$.

Comparing the voltage transformation ratio of the DC converter as shown in Figure 4, the deviation for the DC converter ratio K_1 is $|\Delta K_1| = 0.0134$, and for the DC converter ratio K_2 is $|\Delta K_2| = 0.012$.

Comparing the calculated node voltage magnitudes as shown in Figure 5A, the maximum voltage deviation between the two calculations is $|\Delta U_{\max}| = 0.0139$, with other node voltage deviations not exceeding 0.01. The average relative error in node voltage is $\overline{|\Delta U|} = 1.818 \times 10^{-5}$. Comparing the calculated node voltage phase angles as shown in Figure 5B, the maximum phase

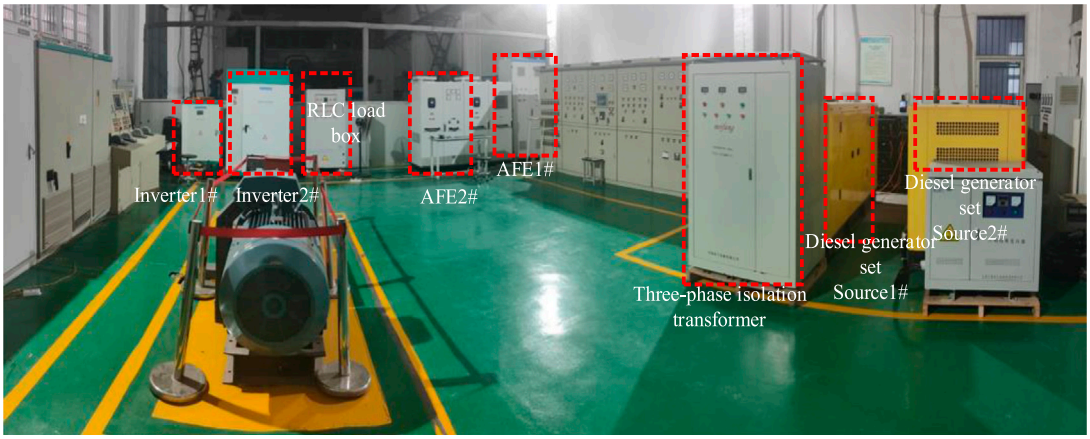

FIGURE 13
Field diagram of the experimental platform.

TABLE 4 Main parameters of the experimental platform.

Parameter	Value
Rated capacity of diesel engine	80 kW
AFE1# Rated capacity	75 kW
AFE2# Rated capacity	259 kW
Inverter 1# rated capacity	250 kW
Inverter 2# rated capacity	50 kW
Maximum capacity of the load box	200 kW
AC line impedance	1.119 + j0.964 Ω/m
DA line resistance	0.521 Ω/m

difference between the two calculations is $|\Delta\vartheta_{max}| = 0.5861°$, with an overall deviation within ±0.6°. The average relative error in node voltage phase angles is $\overline{|\Delta\vartheta|} = 0.17652$.

Based on the simulated results mentioned above, the proposed improved algorithm demonstrates a 80% increase in computational speed while maintaining small computational errors. It meets the requirements of both computational accuracy and efficiency for rapid analysis of microgrids, providing evidence for the feasibility and high computational efficiency of the proposed algorithm.

4 Error analysis

The power flow annotation for the modified IEEE 11-node system structure is shown in Figure 6.

From the power flow illustrated in Figure 6, it is evident that for the hybrid AC/DC system, nodes 3 and 5 involve issues regarding the synthesis and distribution of power between AC and DC systems. In this paper, certain DC parameters in the correction equations during DC power flow computation were removed, leading to relative errors between the actual values and the influx and distribution of DC power at the interface nodes between the DC and AC systems. Figure 7 shows the phase error curve of node voltages. As the electrical distance between nodes and the reference node increases, the phase error of node voltages gradually increases. In multi-node radial networks, an increase in the electrical distance between nodes and the reference node leads to a gradual increase in calculation errors. However, for microgrid systems with lower voltage levels, where the electrical distance between nodes is shorter, the errors generated by the improved algorithm are relatively small.

Comparing Eqs 11, 12, the deviation of active power and reactive power for a single iteration process at a certain node in the system is given by Eq. 13:

$$\begin{cases} \Delta(\Delta P) = \left(\dfrac{\partial \Delta P_a}{\partial \delta_d} + \dfrac{\partial \Delta P_d}{\partial \delta_d}\right)\Delta\delta_d \\ \Delta(\Delta Q) = \Delta Q_d + \dfrac{\partial Q_a}{\partial \delta_d}\Delta\delta_d \end{cases} \tag{13}$$

Analyze the impact of U_i or U_j and $\Delta\delta_d$ on $\Delta(\Delta P)$ and conduct a quantitative analysis. It is observed that the expressions for the partial derivatives of ΔP_a with respect to $\Delta\delta_d$ are consistent with those for ΔP_d. For ease of analysis, $\partial\Delta P_a/\partial\delta_d$ and $\partial\Delta P_d/\partial\delta_d$ are unified as $\partial\Delta P/\partial\delta_d$. Taking node voltage $U_i = U_j$, $G_{ij} + B_{ij} = 5 + j10$, we plot the error influence curves of $\Delta\delta_d$ and U_i on $\partial\Delta P/\partial\delta_d$, as shown in Figure 8, with all variables represented in per unit values. Combining the simulation results, the curves for active power error and node voltage error are plotted separately in Figures 9, 10.

From Figure 8, it can be observed that when U_i remains constant, at lower values of $\Delta\delta_d$, the numerical impact of $\Delta\delta_d$ on $\Delta(\Delta P)$ is relatively small. As the value of $\Delta\delta_d$ increases, the impact on $\Delta(\Delta P)$ gradually increases, and the degree of impact continues to grow without an upper limit. When $\Delta\delta_d$ remains constant, at lower values of U_i, the numerical impact on $\Delta(\Delta P)$ is relatively small. As the value of U_i increases, the impact on $\Delta(\Delta P)$ gradually increases, reaching a maximum degree of impact. The impact curve approximately exhibits a periodic function.

At lower voltage levels, $\Delta(\Delta P)$ is primarily influenced by $\Delta\delta_d$. As both $\Delta\delta_d$ and U_i increase, $\Delta(\Delta P)$ is influenced by both variables with similar degrees of impact. As $\Delta\delta_d$ continues to increase, $\Delta(\Delta P)$

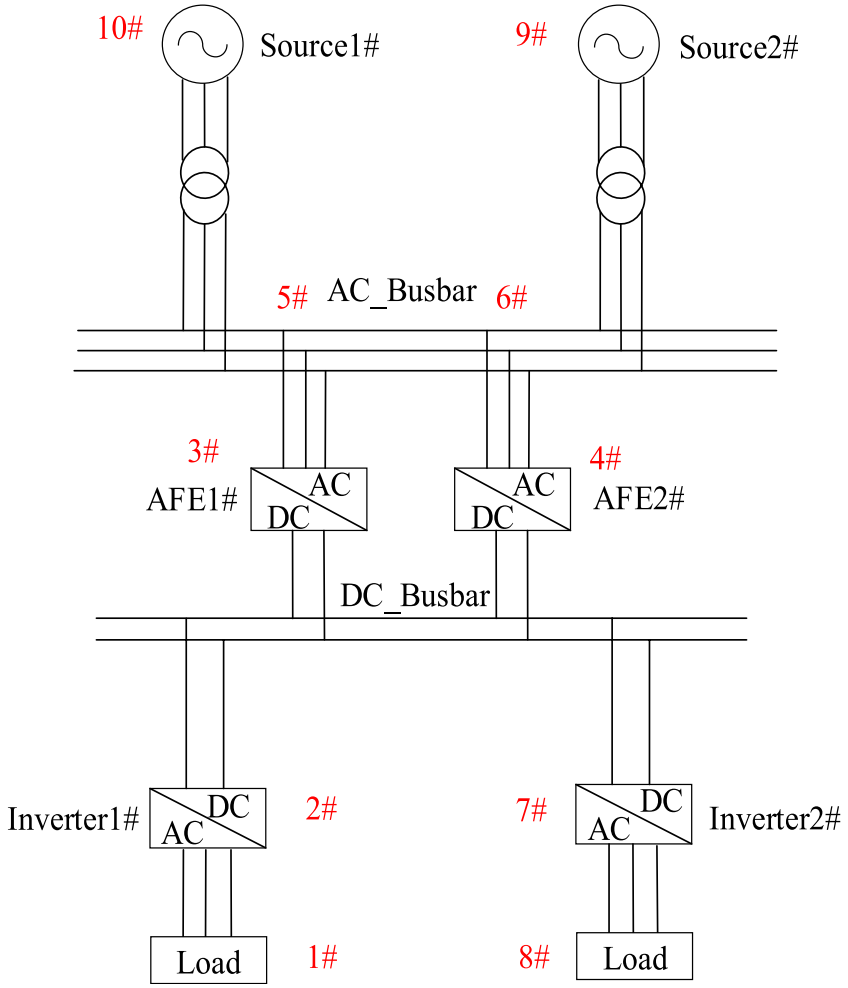

FIGURE 14
System wiring diagram.

is primarily influenced by U_i. In the example, where the voltage phase $\Delta\delta_d$ is relatively small, the impact of U_i on $\Delta(\Delta P)$ is more pronounced compared to $\Delta\delta_d$. This is evident in nodes 3, 5, and 6 where the node voltages have relatively large errors, corresponding to peaks in the active power error curve.

Analyze the impact of ΔQ_d and $\Delta\delta_d$ on $\Delta(\Delta Q)$, we plot the error influence curves of ΔQ_d and $\Delta\delta_d$ on $\Delta(\Delta Q)$ in Figure 11, with all variables represented in per unit values. Combining the simulation results, the reactive power error curve is plotted in Figure 12.

When ΔQ_d remains constant, as the value of $\Delta\delta_d$ increases, the numerical impact on $\Delta(\Delta Q)$ gradually increases, and the degree of impact continues to grow without an upper limit. When $\Delta\delta_d$ remains constant, ΔQ_d consistently has a significant impact on $\Delta(\Delta Q)$. Combining the power flow diagram in Figure 8, for nodes 3 and 5, there is a relationship $\Delta Q = \Delta Q_a + \Delta Q_d$. For lower values of $\Delta\delta_d$, $\Delta(\Delta Q)$ is primarily influenced by ΔQ_d. As $\Delta\delta_d$ increases, $\Delta(\Delta Q)$ is influenced by both variables with similar degrees of impact. As $\Delta\delta_d$ continues to increase, $\Delta(\Delta Q)$ is primarily influenced by $\Delta\delta_d$, and the degree of impact becomes more significant.

Observing Figure 12, it can be noted that there are significant errors in the reactive power on branches with the branch numbers 3, 4, 7, and 9. In the example, where the voltage phase $\Delta\delta_d$ is relatively small, $\Delta(\Delta Q)$ is primarily influenced by ΔQ_d. The lines with significant errors are mainly located at the connection points of DC and AC lines, specifically at nodes 3 and 5. In the iteration process, elements of ΔQ_d in the correction equation for these two nodes were removed, leading to errors in the overall numerical values. Moreover, the closer the lines are to nodes 3 and 5, the larger the errors generated.

For systems with numerous parallel AC and DC lines in the network, the convergence and distribution of AC and DC power flows occur at the connection points. Ignoring ΔQ_d can lead to significant errors in the iterative calculation of reactive power for the system, and the errors increase with more parallel branches. In microgrid systems with a common bus configuration, where there are fewer parallel branches, the overall error in the iterative calculation of reactive power is relatively small.

In summary, $\Delta(\Delta P)$ is primarily influenced by the voltage phase $\Delta\delta_d$ and voltage magnitude U_i. $\Delta(\Delta Q)$ is mainly influenced by $\Delta\delta_d$ and the reactive power

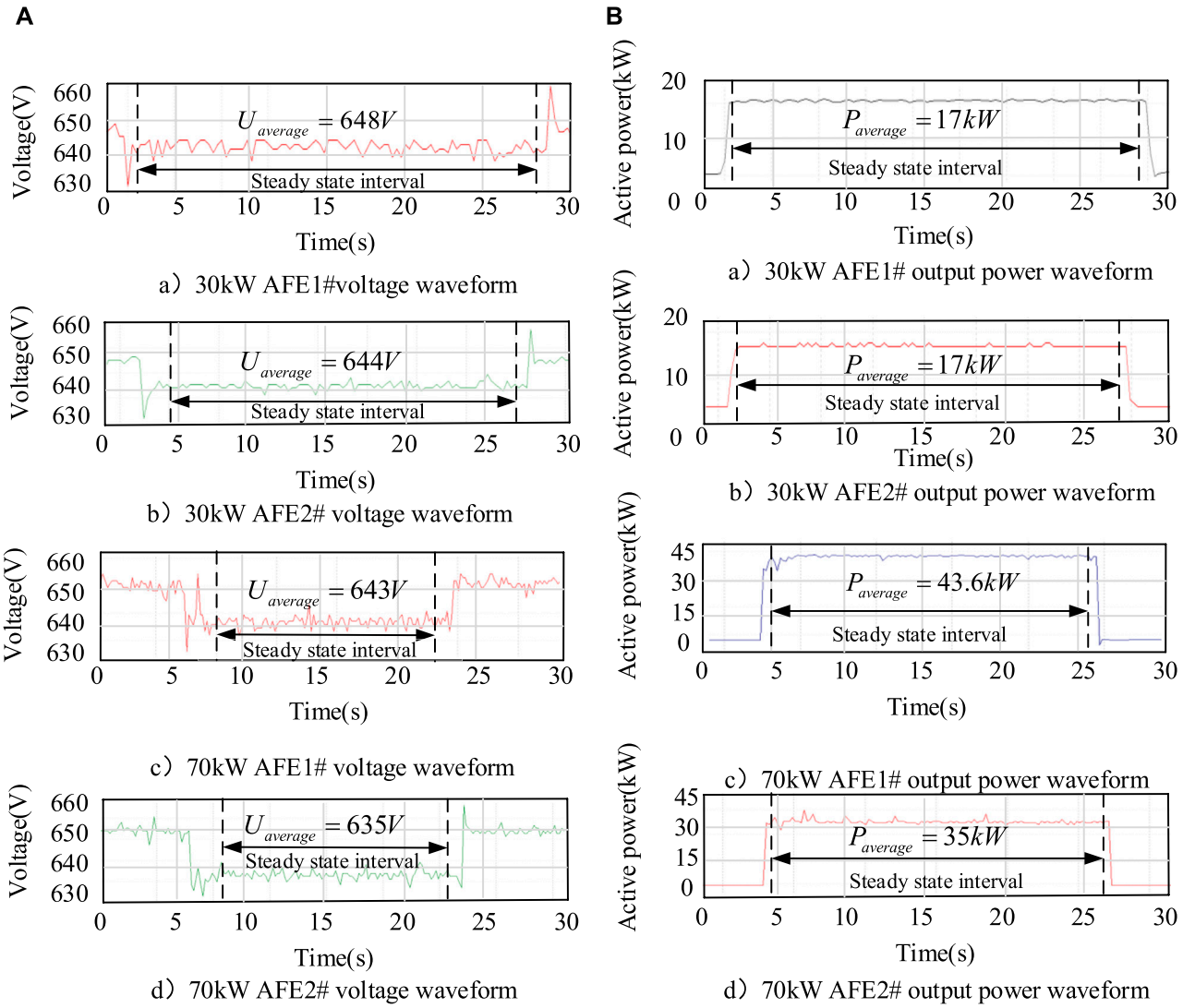

FIGURE 15
Data acquisition results for AFE1# and AFE2#. **(A)** Voltage waveform. **(B)** Power waveform.

TABLE 5 Voltage calculation results and relative errors.

Node number	Voltage under 30 kW load(V)	Voltage under 30 kW load(V)	Relative error under 30 kW load (%)	Relative error under 70 kW load (%)
3	611	636	5.71	1.09
4	610	643	5.28	1.26

TABLE 6 Power calculation results and relative errors.

Node number	Power under 30 kW load (kW)	Power under 30 kW load (kW)	Relative error under 30 kW load (%)	Relative error under 70 kW load (%)
3	17.9	46	5.29	5.5
4	18.7	37.6	10	7.43

imbalance ΔQ_d. When $\Delta\delta_d$ is small, $\Delta(\Delta P)$ is primarily influenced by U_i. When $\Delta\delta_d$ and U_i are large, $\Delta(\Delta P)$ is mainly influenced by $\Delta\delta_d$, and the degree of influence is significant. $\Delta(\Delta Q)$ is primarily influenced by ΔQ_d. At the connection points of AC and DC lines within the mixed AC/DC system, relatively large errors in $\Delta(\Delta Q)$ and node voltage phase can occur.

5 Experimental verification

5.1 Experimental platform

To further validate the feasibility of the proposed improved algorithm, experimental verification was conducted on the experimental platform shown in Figure 13.

Table 4 shows the specific data of the experimental equipment in the experimental platform.

Equivalent the experimental platform to the system wiring diagram as shown in Figure 14, and assign node numbers to the nodes in the system. Set node 10 as the Slack node with $V_{10} = 1.05\angle 0°$ while the remaining nodes are PQ nodes. Perform experimental validation for two operating conditions of load 1#: 30 kW and 70kW, respectively. Write improved power flow algorithm code in MATLAB, input basic data, and calculate the active power and node voltage at the (Analog Front End) AFE1# and AFE2# locations. and connect them to the upper computer. Utilize the system software to monitor the output power and voltage at these two locations, and compare the values with the calculated results.

5.2 Experimental result

The voltage waveforms of AFE1# and AFE2# detected by the upper computer under 30kW and 70 kW loads are shown in Figure 15A. The output power waveforms are illustrated in Figure 15B.

Utilizing the proposed improved algorithm to obtain the current power flow solution for the system, and comparing the calculated values with the steady-state values measured by the upper computer. The error results for different loads are presented in Tables 5, 6.

In summary of the above experimental results, for the 30 kW load experiment, the output power error of Node 4 is 10%, and the errors of other node variables are around 5%. For the 70 kW load experiment, the output power error of Node 4 is 7.43%, the output power error of Node 3 is 5.5%, and the voltage error is around 1%.

Comparing the error results of the two experiments, the voltage error results of AFE1# and AFE2# nodes are basically similar. AFE1# has a relatively smaller output power error compared to AFE2#. According to the error analysis results in Section 4, AFE1# is closer to the load in electrical distance, has a smaller line resistance, and requires relatively fewer iterations throughout the calculation process. Therefore, it generates a relatively smaller relative error.

Based on the experimental validation above, the error range between the overall actual measurements and calculated values is within 10%, ensuring relatively accurate results while maintaining computational speed. This verifies the feasibility of the proposed improved algorithm. Particularly in hybrid AC/DC microgrid systems with short electrical distances, this algorithm demonstrates applicability.

6 Conclusion

This paper, based on the characteristics of DC systems, simplifies the correction equations of the unified iteration method and proposes a power flow calculation model for hybrid AC/DC microgrids based on the improved unified iteration method. The following conclusions can be drawn through theoretical analysis and simulation/experimental verification:

1. By neglecting the flow of reactive power within the DC system and the influence of phase angles on the system, the Jacobian matrix in the correction equations of the unified iteration method is simplified and reduced in order to derive a power flow calculation method for hybrid AC/DC microgrids based on the unified iteration method. The case results indicate that the proposed improved algorithm improves computational speed by 80% compared to the Unified Iterative Method.
2. For the proposed improved algorithm, the error in active power is mainly influenced by the voltage phase angle ($\Delta\delta_d$) and voltage magnitude (U_i), while the error in reactive power is primarily affected by ΔQ_d and $\Delta\delta_d$. When $\Delta\delta_d$ is small, the error in active power is mainly influenced by U_i, and the error in reactive power is primarily affected by ΔQ_d.
3. To experimentally validate the proposed improved algorithm, the magnitude of errors generated for different nodes is related to the electrical distance between the nodes and the load nodes. The longer the electrical distance, the more iterations are required during the power flow calculation process, leading to larger errors.

Data availability statement

The raw data supporting the conclusion of this article will be made available by the authors, without undue reservation.

Author contributions

XD: Writing–original draft, Writing–review and editing. HW: Writing–review and editing. CZ: Writing–review and editing. WY: Writing–review and editing. RY: Writing–review and editing. LX: Writing–review and editing. WL: Writing–review and editing. CL: Writing–review and editing.

Funding

The author(s) declare that financial support was received for the research, authorship, and/or publication of this article. This paper was supported by the National Natural Science Foundation of China (52171308); Natural Science Foundation of Fujian Province, China (2022J01333); Innovation Laboratory for Sciences and Technologies of Energy Materials of Fujian Province and 2022J01813.

Conflict of interest

The authors declare that the research was conducted in the absence of any commercial or financial relationships that could be construed as a potential conflict of interest.

The author(s) declared that they were an editorial board member of Frontiers, at the time of submission. This had no impact on the peer review process and the final decision.

Publisher's note

References

Bajpai, R. S. (2023). An efficient MPC-based Droop control strategy for power sharing in a hybrid AC/DC microgrid using renewable energy resources. *IETE J. Res.*, 1–15. doi:10.1080/03772063.2023.2173664

Chen, H., Zhinong, W., and Shen, H. (2017). Three-term decoupling power flow algorithm for isolated AC-DC hybrid microgrids based on sequence components. *Electr. Power Autom. Equip.* 37 (09), 31–37+45. doi:10.16081/j.issn.1006-6047.2017.09.005

Chen, P., Xiao, X., and Tang, S. (2019). Equivalent Algorithm of interval power flow in AC/DC hybrid distribution Network. *Proc. CSEE* 39 (04), 979–992. doi:10.13334/j.0258-8013.pcsee.180424

Guoqing, L., Jing, B., and He, W. (2017). Review on DC grids power flow analysis and control. *High. Volt. Eng.* 43 (4), 1067–1078. doi:10.13336/j.1003-6520.hve.201700328002

Hameed, F., Ai Hosani, M., and Zeineldin, H. H. (2019). A modified backward/forward sweep load flow method for islanded radial microgrids. *J. Technol.* 10 (1), 910–918. doi:10.1109/tsg.2017.2754551

Heidary, J., Gheisarnejad, M., and Khooban, M. H. (2023). Stability enhancement and energy management of AC-DC microgrid based on active disturbance rejection control. *Electr. Power Syst. Res.* 217, 109105–109113. doi:10.1016/j.epsr.2022.109105

Huang, Y., Ai, X., Fang, J., Cui, S., Zhong, R., Yao, W., et al. (2023). Holomorphic embedding power flow modeling of autonomous AC/DC hybrid microgrids. *Int. J. Electr. Power and Energy Syst.* 145, 108549. doi:10.1016/j.ijepes.2022.108549

Ju, Y., Liu, W., Zhang, Z., and Zhang, R. (2022). Distributed three-phase power flow for AC/DC hybrid networked microgrids considering converter limiting constraints. *IEEE Trans. Smart Grid* 13, 1691–1708. doi:10.1109/tsg.2022.3140212

Lee, J.-Oh, Kim, Y.-Su, and Moon, S.-ll (2020). Current injection power flow analysis and optimal generation dispatch for bipolar DC microgrids. *IEEE Trans. Smart Grid* 12, 1918–1928. doi:10.1109/TSG.2020.3046733

Li, Z., Xie, X., Cheng, Z., Zhi, C., and Si, J. (2023). A novel two-stage energy management of hybrid AC/DC microgrid considering frequency security constraints. *Int. J. Electr. Power and Energy Syst.* 146, 108768. doi:10.1016/j.ijepes.2022.108768

Lin, L., Dong, S., and Zhu, C. (2020). Power flow calculation of isolated island microgrid based on two-step solution of cofactor. *Power Grid Technol.* 44 (10), 3955–3963. doi:10.13335/j.1000-3673.pst.2019.1942

Liu, K., Chun, W., and Wu, H. (2019b). A method for calculating linear power flow in distribution network with PV nodes. *Power Syst. Prot. Control* 47 (03), 17–22.

Liu, K., Wang, C., and Chen, Y. J. (2019a). Linear power flow calculation of distribution networks with distributed generation. *IEEE Access* (7), 44696–44695. doi:10.1109/ACCESS.2019.2909325

Liu, Y., Li, Z., and Fan, M. (2021). A Newton-Raphson-Based sequential power flow algorithm for hybrid AC/DC microgrids. *IEEE Trans. Industry Appl.* 58, 843–854. doi:10.1109/tia.2021.3123246

Nejabatkhah, F., Yunwei, L., and Hao, T. (2019). Power quality control of smart hybrid AC/DC microgrids: an overview. *IEEE Access* 7, 52295–52318. doi:10.1109/access.2019.2912376

Peng, H., Shuaihu, L., Hui, L., and Huang, X. (2017). Power Flow calculation of AC-DC hybrid microgrids operating in isolatedislands. *Power Grid Technol.* 41 (09), 2887–2896. doi:10.13335/j.1000-3673.pst.2017.0379

Pengfei, L. V. (2022). Research on HVDC operation characteristics under influence of hybrid AC/DC power grids. *Power Syst. Technol.* 46 (02), 503–510. doi:10.13335/j.1000-3673.pst.2021.2403

Song, L., Jianwei, L., and Dong, Y. (2021). Flexible power control and voltage suppression strategy for multi-sub-microgrid AC-DC hybrid distribution system. *Electr. Power Autom. Equip.* 41 (05), 99–106. doi:10.16081/j.epae.202105030

Song, Z., Yaohui, H., and Zhao, H. (2023). Applicability analysis of power flow calculation method for AC-DC hybrid power network with multiple types of DC [J/OL]. *Electr. Power Autom. Equip.*, 1–10. doi:10.16081/j.epae.202307004

Wang, J., Xin, A., Wang, K., and Li, R. (2018). A new AC-DC decoupling power flow algorithm based on Augmented Jacobian Matrix. *Trans. China Electrotech. Soc.* 33 (06), 1382–1389. doi:10.19595/j.cnki.1000-6753.tces.170277

Wang, X., Peng, C., and Sun, H. (2023). Power flow calculation for AC-DC hybrid power networks considering VSC control strategy. *Proc. CSEE* 43 (10), 3731–3742. doi:10.13334/j.0258-8013.pcsee.212339

Yang, G. K., Dong, P., Liu, M., and Wu, H. (2021). Research on random fuzzy power flow calculation of AC/DC hybrid distribution network based on unified iterative method. *IET Renew. Power Gener-ation* 15, 731–745. doi:10.1049/rpg2.12063

Yang, Z. F., Xie, K. G., Yu, J., Zhong, H., Zhang, N., and Xia, Q. X. (2019). A general formulation of linear power flow models: basic theory and error analysis. *IEEE Trans. Power Syst.* 34 (2), 1315–1324. doi:10.1109/tpwrs.2018.2871182

Zhu, L., Rong, X., Zhao, J., Zhang, H., Zhang, H., Jia, C., et al. (2022). Topology optimization of AC/DC hybrid distribution network with energy router based on power flow calculation. *Energy Rep.* 8, 1622–1638. doi:10.1016/j.egyr.2022.02.208

Zou, Z., Wang, C., and Zhang, C. (2022). Linear power flow calculation of isolated island microgrid based on sag control. *Laboratory Res. Explor.* 41 (05), 124–129. doi:10.19927/j.cnki.syyt.2022.05.027

10.3389/fenrg.2024.1376714

Nomenclature

UIM	unified iteration method
IUIM	improved unified iteration method
DPF	Distributed Power Flow
ALADIN	Augmented Lagrangian Alternating Direction Inexact Newton
Variable annotation table	
Variable	Notes
E_r、 E_i	Rectifier side and inverter side AC voltage
U_{dor}、 U_{doi}	Ideal no-load DC voltage of rectifiers and inverters
$U_{dor}\cos\alpha$ $U_{doi}\cos\beta$	The ideal no-load DC voltage of rectifier and inverter after the commutation process
α、 β	Rectifier trigger angle and inverter extinction angle
d_{xr}、 d_{xi}	Equivalent impedance of rectifier and inverter
U_{dr}、 U_{di}	Output voltage at the terminals of rectifier and inverter
P_{dr}、 P_{di}	Terminal power of rectifier and inverter
I_d、 P_d、 R_1	DC line Current, active power and equivalent resistance
ΔP_i、 ΔQ_i	Active power and reactive power imbalance at node i
P_i、 Q_i	Active power and reactive power injected into node i
U_i、 U_j	Voltage magnitudes at nodes i and j
G_{ij}、 B_{ij}	Real and imaginary parts of Admittance Y_{ij} between nodes i and j
δ_{ij}	Phase difference between nodes i and j
φ_k	Power factor angle of the converter
ΔP_a、 ΔQ_a ΔP_d、 ΔQ_d	Active power and reactive power imbalance at AC/DC flow nodes
J	Jacobian matrix
K_r、 K_i	Turns ratio of converter transformers on rectifier and inverter sides
θ_d	Converter control angle $\omega_d = \cos\theta_d$
$\Delta(\Delta P)$、 $\Delta(\Delta Q)$	Error in active (reactive) power imbalance